Journal of
Synchrotron Radiation

ISSN 0909-0495

Received 7 May 2012
Accepted 29 July 2012

X-ray velocimetry within the *ex vivo* carotid artery

R. A. Jamison,[a,b] K. K. W. Siu,[c,d] S. Dubsky,[a,b] J. A. Armitage[e] and Andreas Fouras[a,b]*

[a]Division of Biological Engineering, Monash University, Victoria 3800, Australia, [b]Department of Mechanical and Aerospace Engineering, Monash University, Victoria 3800, Australia, [c]Australian Synchrotron, Clayton, Victoria 3168, Australia, [d]Monash Biomedical Imaging and School of Physics, Monash University, Victoria 3800, Australia, and [e]Department of Anatomy and Developmental Biology, School of Biomedical Sciences, Monash University, Victoria 3800, Australia. E-mail: andreas.fouras@monash.edu

X-ray velocimetry offers a non-invasive method by which blood flow, blood velocity and wall shear stress can be measured in arteries prone to atherosclerosis. Analytical tools for measuring haemodynamics in artificial arteries have previously been developed and here the first quantification of haemodynamics using X-ray velocimetry in a living mammalian artery under physiologically relevant conditions is demonstrated. Whole blood seeded with a clinically used ultrasound contrast agent was pumped with a steady flow through live carotid arterial tissue from a rat, which was kept alive in a physiological salt solution. Pharmacological agents were then used to produce vascular relaxation. Velocity measurements were acquired with a spatial resolution of 14 μm × 14 μm and at a rate of 5000 acquisitions per second. Subtle velocity changes that occur are readily measurable, demonstrating the ability of X-ray velocimetry to sensitively and accurately measure haemodynamics *ex vivo*. Future applications and possible limitations of the technique are discussed, which allows for detailed living tissue investigations to be carried out for various disease models, including atherosclerosis and diabetic vasculopathy.

Keywords: phase contrast; X-ray velocimetry; blood flow; *ex vivo* imaging; particle image velocimetry.

1. Introduction

The ability to accurately measure blood flow and shear within living tissue is essential to increasing our understanding of cardiovascular disease, which is estimated to cause 58% of all deaths across the globe (Mendis *et al.*, 2011). The fluidic forces from blood are transferred to the vessel walls as shear, *via* the endothelial cells, the innermost cellular layer of the blood vessel that lines the vessel lumen. Endothelial tissue acts as an active barrier to the tissue beneath through its ability to generate biological effectors, such as vasoactive substances, procoagulants and anticoagulants (Gimbrone, 1999). Indeed, endothelial damage is central to the aetiology of cardiovascular disease including atherosclerosis. Although endothelial cells experience arterial pressure, flow and shear forces, it is thought that wall shear stress is the primary stimulus to endothelial cell activation and the release of vasoactive substances or chemokines. It is now widely recognized that wall shear stress (WSS) plays the most fundamental role in atherosclerosis (Chatzizisis *et al.*, 2007; Feldman *et al.*, 2002; Jamison *et al.*, 2012*a*). As a result, significant effort is being directed towards detailing the biological consequences of altered WSS (Cheng *et al.*, 2006; Conklin *et al.*, 2002; Gertz & Roberts, 1990), in particular those areas most prone to low WSS (Baek *et al.*, 2009; Shojima *et al.*, 2004).

Unfortunately, WSS is a difficult quantity to measure (Vennemann *et al.*, 2007) and is often estimated by measuring the velocity at a single point in space, then assuming that the flow present is parabolic. This assumption is an over-simplification of the true flow and omits consideration of the complex cardiovascular geometry and the pulsatile nature of blood flow, both of which are known to result in non-parabolic flow profiles (Bulwer & Rivero, 2009). Alternatively, the WSS can be accurately measured experimentally if the full field velocity profile is known. Wall shear stress is derived from the wall-normal derivative of velocity and the viscosity, defined as $\mathrm{WSS} = \mu\, \mathrm{d}v/\mathrm{d}n$, where μ is the dynamic viscosity, v is the velocity parallel to the wall and n is the coordinate normal to the wall.

A number of techniques allow for the measurement of *in vivo* whole-field blood velocity, including particle image velocimetry (PIV), magnetic resonance imaging (MRI), ultrasound, laser Doppler and laser speckle techniques. While MRI and ultrasound are widely used clinically, neither allow

for the combination of high spatial and temporal resolution required to resolve blood flow across a blood vessel and throughout the cardiac cycle, as needed for this study. PIV (Adrian, 1991, 2005) is an imaging method recognized as one of the most capable techniques for acquiring velocity measurements at the spatial and temporal resolutions required for accurate WSS measurements (Vennemann *et al.*, 2007). PIV requires a pair of images of a seeded flow to be acquired at a specified time interval. The images are divided into integration windows and cross correlation is utilized to determine the modal displacement of all particles within the interrogation window; this, combined with the known time interval, gives the instantaneous velocity. Unfortunately the opacity of living tissue renders visible-light-based imaging methods unable to assess internal fluid dynamics, such as in the deep vasculature.

X-ray velocimetry (Lee & Kim, 2003; Fouras *et al.*, 2007*a*, 2009*a*), a novel variant of standard PIV, allows the investigation of optically opaque specimens, overcoming the restriction of optical access. As an enhancement of conventional X-ray absorption imaging, propagation-based X-ray phase-contrast imaging (PCI) (Cloetens *et al.*, 1996; Davis *et al.*, 1995; Snigirev *et al.*, 1995) utilizes a long propagation distance between the sample and the detector. This distance allows the X-rays that are refracted when passing though the sample to interfere at the detector with those incident X-rays that passed directly through the sample. This technique produces a characteristic edge enhancement that serves to also increase contrast and hence signal-to-noise ratio. Recent studies demonstrating the ability of X-ray velocimetry to measure the WSS of blood flow *in vitro* (Jamison *et al.*, 2011) identifies it as a possible tool in the investigation of haemodynamic forces *in vivo*. Previous X-ray velocimetry studies on whole blood without the addition of tracer particles have been successful by utilizing phase-contrast imaging (Irvine *et al.*, 2008; Kim & Lee, 2006; Lee & Kim, 2005); however, the relatively small phase difference between red blood cells and the surrounding tissue renders this technique impractical for *in vivo* studies (Jamison *et al.*, 2011). Our group therefore uses a clinical ultrasound contrast agent seeded in whole blood (Dubsky *et al.*, 2010). This agent consists of lipid-coated air micro-bubbles that have high X-ray contrast.

While laser-based PIV has previously been conducted *in vivo* for small transparent vessels found in rodents (Smith *et al.*, 2003; Sugii *et al.*, 2002.), chicken embryos (Lee *et al.*, 2007; Poelma *et al.*, 2010; Vennemann *et al.*, 2006) and zebrafish embryos (Forouhar *et al.*, 2006; Hove *et al.*, 2003; Jamison *et al.*, 2012*b*), *in vivo* haemodynamic studies within similar models have yet to be achieved using X-ray velocimetry. A recent study has successfully utilized X-ray imaging to estimate a flow field by manually identifying 48 individual particle streaks from 100 images (Jung *et al.*, 2012). Here we investigate whole blood flow, seeded with contrast agent, within an extracted rat common carotid artery, delivering ~12000 independent measurements across an image sequence of 2000 images, and demonstrating the next advance in X-ray velocimetry. Our protocol enables investigation of haemodynamics in a setting typical of an *in vivo* environment whilst omitting the noise from the surrounding tissue. This allows for the quantification of flow and WSS within vessels that retain the complexities of living tissue, using a contrast agent that is fully biocompatible and approved for use in human diagnostics.

2. Method and results

2.1. Flow set-up

Whole blood seeded with contrast agent was pumped through the flow loop consisting of a pair of glass cannulae upon which the living artery was mounted, a peristaltic pump and a flow probe all connected *via* silicone tubing (see Fig. 1). A clinical ultrasound contrast agent, DEFINITY (Bristol-Myers Squibb Medical Imaging), was used to increase the signal-to-noise ratio without adversely affecting the properties of the blood. When activated, DEFINITY produces a homogeneous injectable suspension of biocompatible perflutren lipid microspheres encapsulating micro-bubbles of air. It is primarily used clinically for suboptimal echocardiograms to opacify the left ventricular chamber and improve the delineation of the left ventricular endocardial border. DEFINITY was remotely injected into the flow loop upstream of the vessel chamber by a micro-syringe pump (WPI, UMP2) at a rate of 5 $\mu L\ s^{-1}$ for 20 s (representing approximately 1.2×10^9 micro-bubbles per ml of blood). This was performed at a distance upstream that allowed sufficient time for the contrast agent to be incorporated into the flow. A peristaltic pump (Walker P720/66) was used to circulate the blood though the system while a riser tube allowed for accurate selection of the pressure within the flow system. The flow rate was chosen to

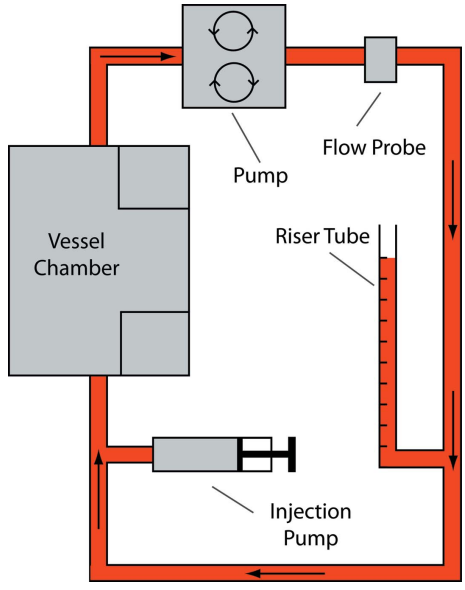

Figure 1
Schematic diagram of the flow loop used. The vessel chamber holds the artery and blood is circulated through the system by the pump. The probe independently measures the flow while the riser tube and injection pump set the mean pressure and allow for injection of contrast agent, respectively.

be 0.15 mL min^{-1} and the mean pressure of the system was set at 100 mmHg to mimic the conditions found *in vivo*. Although the peristaltic pump produces a pulsatile flow, owing to the nature of its design (positive displacement achieved by rollers), pumping at an extremely low frequency is seen to produce a near steady flow. A flow probe (Transonic Systems, TS410 transit-time tubing flowmeter with a 1PXN flow probe) was used to independently measure the flow rate of the system and a data acquisition module (IDT MotionPro) was used to record the data. The flow probe was unable to be used with the blood seeded with DEFINITY. Consequently, flow data were acquired immediately before injecting the contrast agent.

2.2. Vessel mounting and preparation

The tissue bath and mixing bath for these experiments are shown in Fig. 2. A commercially available tissue bath (Living Systems) was modified to allow for vertical mounting of samples to enable X-ray imaging with illumination from a horizontally aligned synchrotron beam. The bath is designed to rest on a rotation stage such that the tissue sample is aligned directly with the centre of the stage (allowing for minimal translation of the tissue during rotation). The tissue bath consists of an isolated line for blood flow and additional inlets and outlets to circulate the fluid surrounding the vessel. The blood line has two internal glass cannulae for attachment of the blood vessel. Each cannula is held in position by a Teflon clamp. The clamps are permanently aligned in one axis, while the other two axes are fully adjustable from the controls on the exterior of the chamber, allowing for easy alignment during vessel mounting and precise adjustment for imaging. Situated within the tissue bath is a temperature sensor (Living Systems) that connects to a custom-made temperature-monitoring system capable of controlling the heater element, allowing accurate temperature control. The heating element of the temperature controller is located in a custom-made Teflon mixing bath, ensuring that bubbles generated at the heater element do not enter the tissue bath. The mixing bath also allows oxygenation of the tissue bath medium and for mixing of vasodilators or vasoconstrictors, if required. Mixing can be enhanced through the use of a magnetic stirrer if required.

A rat (Sprague Dawley) was humanely killed and the common carotid artery excised and immediately placed in ice-cold Krebs buffer [Krebs-Henseleit Buffer (Sigma K3753-10L) 9.6 g L^{-1} + 0.373 g L^{-1} $CaCl_2$; pH ∼7.2]. This keeps the vessel alive but the cold temperature slows the metabolic rate and minimizes cell death during dissection and mounting on glass cannulae. The vessel was cleaned of fat and then connected to the glass cannulae by use of fine suture ties in the tissue bath; then the bath was warmed to 310 K in order to return the vessel to normal metabolism. Following imaging of the normal condition, vasodilator was added to the tissue bath medium [2 m*M* sodium nitroprusside, Sigma Aldrich] and the imaging sequence was repeated.

2.3. Imaging

The experiments in this study were performed at the SPring-8 third-generation synchrotron, Hyogo, Japan. The upstream hutch of the medical imaging undulator beamline, 20XU, was used and the broadband synchrotron radiation was filtered by a Si(111) double-crystal monochromator to provide a beam energy of 33 keV. The source-to-sample distance was 80 m and the sample-to-detector distance was 140 cm.

The basic imaging configuration required for X-ray velocimetry is shown in Fig. 3. The water bath was fitted with an imaging window that penetrates the tissue bath with allowance for depth adjustment to minimize the path length of the X-rays and hence absorption by water volume. A modified beam monitor (Hamamatsu AA50) was used to convert the X-rays into visible light using a 23 µm-thick LSO (Lu_2SiO_5:Ce) scintillator. A 10× objective lens (Nikon Brightfield CFI Plan Apo 10×/0.45) was coupled with the detector to obtain an effective pixel size of 0.9 µm × 0.9 µm. The spatial resolution of this system was designed to ensure accurate imaging of the

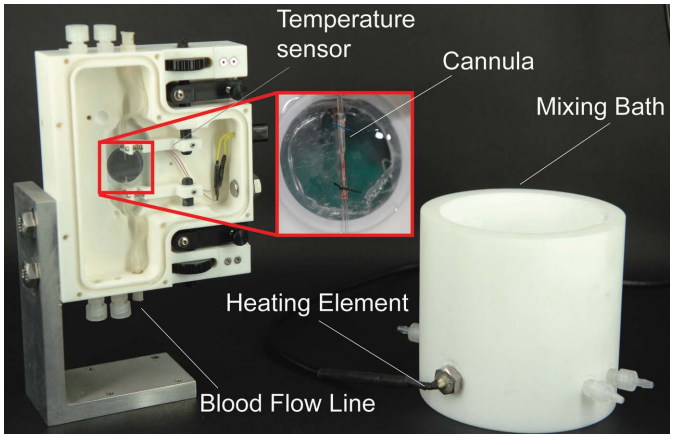

Figure 2
Photographic image of the tissue bath and mixing bath used. The insert shows a close-up of an aorta attached to the cannulae. For reference the cannulae are 1 mm in diameter.

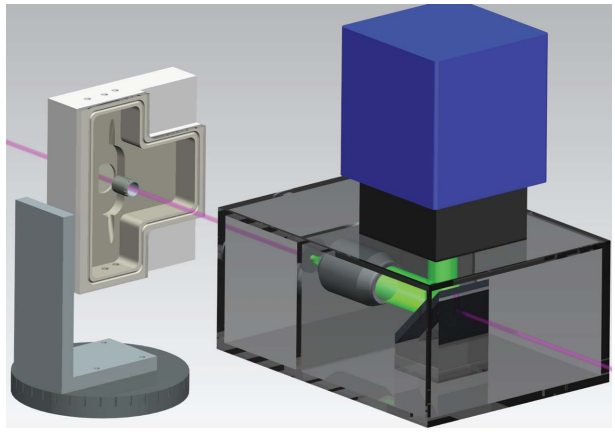

Figure 3
Schematic set-up of the micro X-ray velocimetry configuration. The X-ray beam (purple) penetrates the sample (common carotid artery mounted in the tissue bath) and interacts with the scintillator to produce visible light (green). An objective lens is used to magnify and focus the visible light from the scintillator onto the sensor of the camera. A mirror is used to remove the camera from the X-ray path. For reference, the X-ray beam size is 0.8 mm high × 1.8 mm wide.

air-filled lipid microspheres, which have a mean diameter of 3 μm. The beam size at the sample was approximately 0.8 mm × 1.8 mm.

In order to achieve the temporal resolution required, a high-speed camera (Photron FASTCAM SA2, Tokyo, Japan) was mounted on a Generation3 image intensifier (Lambert II18 Gen3, Roden, The Netherlands). A region of interest was set at 512 pixels × 1536 pixels corresponding to the size of the vessel illuminated by the X-ray beam, enabling cinematic acquisition at a rate of 5000 frames s^{-1}. The intensifier was set to an exposure of 100 μs and a multi-channel plate voltage (gain) of 650 V DC. This reduction of the exposure time to 100 μs is a fivefold improvement compared with previously published haemodynamic investigations using synchrotron radiation (Jamison *et al.*, 2011), signifying a greater capacity to measure high-speed flows. Although a further increase in frame rate is possible (an exposure of 100 μs equates to a maximum possible frame rate of 10000 frames s^{-1}), previous studies have shown that decreasing the ratio of exposure to interframe time (time between frame acquisitions) is detrimental to the accuracy of the results (Fouras *et al.*, 2007*a*).

2.4. Filtering

Owing to the non-uniform illumination provided by the source, unwanted spatial gradients of intensity exist in the image. Removal of the unwanted spatial gradients is achieved by normalizing each pixel row and column by the average intensity of that row or column. This is effective in preventing the effects of the oval profile of the X-ray beam from biasing the cross-correlation process during PIV. Following this spatial filtering, a temporal filter was applied to the images, removing any stationary structures from the image. This is performed by subtracting the temporally averaged image from each of the original images with a time base of 100 ms.

2.5. Particle image velocimetry

The velocity measurements in this study were performed using code developed in-house (Fouras *et al.*, 2008). This code has been developed over a number of years and has been rigorously validated (Fouras *et al.*, 2009*b*; Nesbitt *et al.*, 2009). The uncertainty of displacements measured using this code has been found to be as low as 0.05 pixels (Fouras *et al.*, 2007*b*). Whole-field velocity measurements were carried out on the blood flow through the excised vessel after performing the above-mentioned filtering. The measurements are two-dimensional, with the cross-correlation providing the modal velocity, which, for parabolic-like flows, can be assumed to be at the center of the vessel (Fouras *et al.*, 2007*a*). Interrogation windows of 14 μm × 14 μm were used with a measurement spacing of 7 μm. Owing to the steady nature of the flow, measurements were temporally averaged using a recently developed method called hybrid averaging (Samarage *et al.*, 2012). Hybrid averaging combines the ordinary averaging of velocity vectors with the common practice employed in PIV of averaging cross-correlation maps before evaluating vectors (Meinhart *et al.*, 2000). The hybrid process was shown to give optimal results for this work.

Fig. 4 shows the full-field velocity measurements acquired within the living aorta for both the normal and dilated conditions. As can be clearly seen, the size of the aorta is

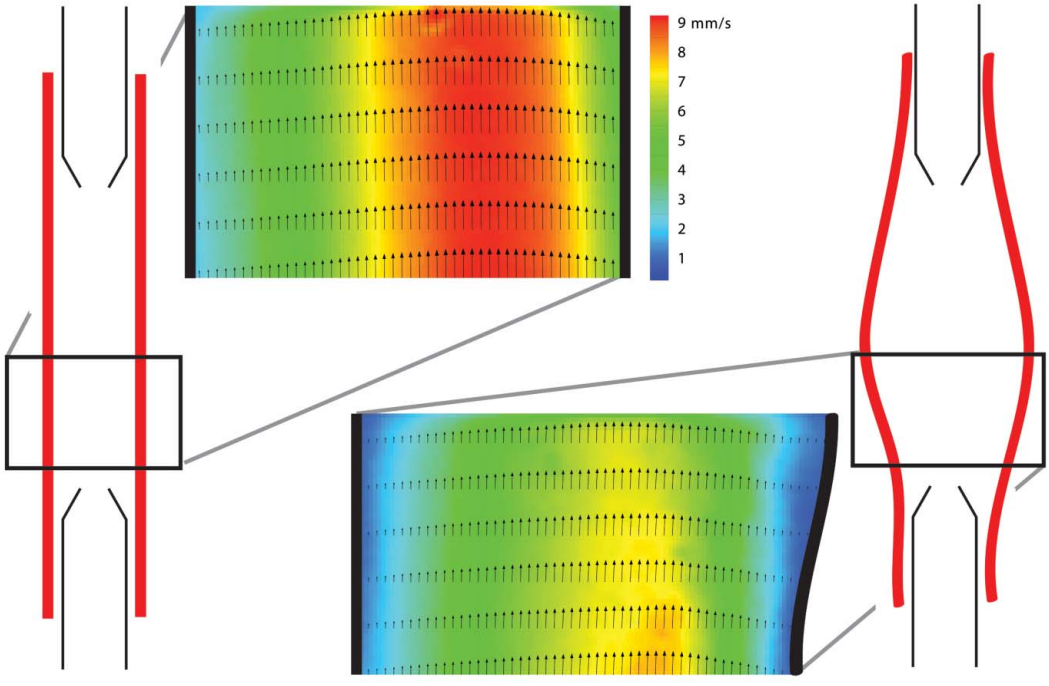

Figure 4
Time-averaged X-ray velocimetry measurements for both the normal (top) and dilate (bottom) condition. Vectors show the direction and magnitude of flow while overlaid contours show velocity magnitude. Vectors are calculated at 7 μm spacing. For clarity only every tenth vector is shown in the vertical direction and every second in the horizontal direction.

significantly altered by the addition of the vasodilator, with an average increase in vessel diameter of ~13%, representing an average increase in area of ~27%. Moreover, the dimensions of the vessel expanded asymmetrically, producing distortions to the previously uniform radius of the vessel along its length. This artifact is produced because the imaging location of the vessel was not in the middle of the cannulae pair but was closer to one cannula, where the suture restricts vessel expansion. The velocity in the dilated vessel is seen to be substantially lower (~24%) than that in the non-dilated vessel. This reduction in velocity results from the expansion of the vessel while maintaining the same flow rate (within 3%). A previously described flow estimation technique (Jamison *et al.*, 2011) that utilizes the additional assumption of axisymmetry was used to determine the flow rate. The measurements agree to within 10% with the initial flow probe readings taken before the addition of DEFINITY (0.136 mL min^{-1} with PIV).

3. Discussion and conclusions

This study is the first demonstration of the capability of X-ray velocimetry to measure complex haemodynamics within living mammalian vasculature. The method employed allowed pharmacological stimulation to alter the physical condition of the vessel. Altered haemodynamics were observed, with the reduction in measured velocity corresponding to the increase in vessel size. This technique allows for detailed living tissue investigations to be carried out in the future, furthering our knowledge in the field of haemodynamics.

As a direct result of the significant improvements of X-ray velocimetry for haemodynamics over the past five years, the ability to accurately measure velocity in mammalian models at high spatial and temporal resolution *in vivo* is fast becoming a reality. The major limiting factor is the ability to measure haemodynamics at physiologically realistic flows and velocities (maximum flow during systole of 17 mL min^{-1} within the rat carotid). Nonetheless, we show that measurements of flow rates up to 0.136 mL min^{-1} are possible.

Increased imaging rates will require an increase in flux, or an increase in detector sensitivity. A significant restriction in the current study is the use of a perfect crystal monochromator with a small bandpass of approximately $\Delta E/E = 10^{-4}$ (Yabashi *et al.*, 1999) on the SPring-8 BL20XU beamline. The use of a higher-bandpass monochromator, *e.g.* Tsuruta *et al.* (1998) and Sawhney *et al.* (2011), could increase the flux reaching the specimen by several orders of magnitude and proportionately increase the flow rate capable of being measured. Such an increase in flux would not correspond to any increase in dose, as the exposure time would be decreased in direct proportion to the increased flux through a high-speed shutter, for example Chua *et al.* (2010) and Lee *et al.* (2009).

While the ability to measure velocity and shear *ex vivo* can increase understanding of disease models, the ability to measure flow *in vivo* is still the ultimate goal for X-ray velocimetry. Interference from overlying tissue is intrinsic to *in vivo* measurements and compounds the difficulty of obtaining velocity measurements since the signal-to-noise ratio is reduced while increasing exposure times (for the same image intensity), with correspondingly slower imaging rates. While stationary structures can be easily removed using the techniques described here, removal of dynamic objects is more difficult. Furthermore, the decrease in signal-to-noise ratio owing to the surrounding tissue will make selection of optimal particulate contrast agents vital. This study has used a clinically available contrast agent; however, other studies have begun developing other biocompatible tracers (Lee *et al.*, 2010; Ahn *et al.*, 2011*a*, 2011*b*). While some difficulties still remain in achieving *in vivo* measurements using X-ray velocimetry, the continual progression of the technique ensures that reaching this milestone is inevitable.

JAA is a Monash Fellow and AF an NHMRC Career Development Fellow. The authors gratefully acknowledge the support of the Japan Synchrotron Radiation Research Institute (JASRI) (under Proposal No. SP2011B1480). The authors would like to thank Yoshio Suzuki, Akihisa Takeuchi and Kentaro Uesugi (SPring-8/JASRI) for their assistance with the experiments. The researchers were also supported by an ISAP grant from the Australian Synchrotron.

References

Adrian, R. J. (1991). *Annu. Rev. Fluid Mech.* **23**, 261–304.
Adrian, R. J. (2005). *Exp. Fluids*, **39**, 159–169.
Ahn, S., Jung, S. Y., Lee, J. P. & Lee, S. J. (2011*b*). *J. Phys. Chem. B*, **115**, 889–901.
Ahn, S., Jung, S. Y., Seo, E. & Lee, S. J. (2011*a*). *Biomaterials*, **32**, 7191–7199.
Baek, H., Jayaraman, M. V. & Karniadakis, G. E. (2009). *Ann. Biomed. Eng.* **37**, 2469–2487.
Bulwer, B. & Rivero, J. (2009). *Echocardiography Pocket Guide: The Transthoracic Examination*, pp. 45–78. Sudbury: Jones and Bartlett.
Chatzizisis, Y. S., Coskun, A. U., Jonas, M., Edelman, E. R., Feldman, C. L. & Stone, P. H. (2007). *J. Am. Collect. Cardiol.* **49**, 2379–2393.
Cheng, C., Tempel, D., van Haperen, R., van der Baan, A., Grosveld, F., Daemen, M. J., Krams, R. & de Crom, R. (2006). *Circulation*, **113**, 2744–2753.
Chua, C. S., Higgins, S. P. A. & Fouras, A. (2010). *J. Synchrotron Rad.* **17**, 624–630.
Cloetens, P., Barretty, R., Baruchely, J., Guigayz, J. & Schlenkerz, M. (1996). *Appl. Phys.* **29**, 133–146.
Conklin, B. S., Zhong, D. S., Zhao, W., Lin, P. H. & Chen, C. (2002). *J. Surg. Res.* **102**, 13–21.
Davis, T. J., Gao, D., Gureyev, T. E., Stevenson, A. W. & Wilkins, S. W. (1995). *Nature (London)*, **373**, 595–598.
Dubsky, S., Jamison, R. A., Irvine, S. C., Siu, K. K. W., Hourigan, K. & Fouras, A. (2010). *Appl. Phys. Lett.* **96**, 023702.
Feldman, C. L., Ilegbusi, O. J., Hu, Z., Nesto, R., Waxman, S. & Stone, P. H. (2002). *Am. Heart J.* **143**, 931–939.
Forouhar, A. S., Liebling, M., Hickerson, A., Nasiraei-Moghaddam, A., Tsai, H. J., Hove, J. R., Fraser, S. E., Dickinson, M. E. & Gharib, M. (2006). *Science*, **312**, 751–753.
Fouras, A., Dusting, J. & Hourigan, K. (2007*b*). *Exp. Fluids*, **42**, 799–810.
Fouras, A., Dusting, J., Lewis, R. & Hourigan, K. (2007*a*). *J. Appl. Phys.* **102**, 064916.
Fouras, A., Kitchen, M. J., Dubsky, S., Lewis, R. A., Hooper, S. B. & Hourigan, K. (2009*a*). *J. Appl. Phys.* **105**, 102009.
Fouras, A., Lo Jacono, D. & Hourigan, K. (2008). *Exp. Fluids*, **44**, 317–329.

Fouras, A., Lo Jacono, D., Nguyen, C. V. & Hourigan, K. (2009*b*). *Exp. Fluids*, **47**, 569–577.
Gertz, S. D. & Roberts, W. C. (1990). *Am. J. Cardiol.* **66**, 1368–1372.
Gimbrone, M. A. (1999). *Thromb. Haemost.* **82**, 722–726.
Hove, J. R., Köster, R. W., Forouhar, A. S., Acevedo-Bolton, G., Fraser, S. E. & Gharib, M. (2003). *Nature (London)*, **421**, 172–177.
Irvine, S. C., Paganin, D. M., Dubsky, S., Lewis, R. A. & Fouras, A. (2008). *Appl. Phys. Lett.* **93**, 153901.
Jamison, R. A., Armitage, J. A., Carberry, J., Kitchen, M. J., Hooper, S. B. & Fouras, A. (2012*a*). *Curr. Pharm. Biotech.* **13**, 2128–2140.
Jamison, R. A., Dubsky, S., Siu, K. K., Hourigan, K. & Fouras, A. (2011). *Ann. Biomed. Eng.* **39**, 1643–1653.
Jamison, R. A., Fouras, A. & Bryson-Richardson, R. J. (2012*b*). *J. Biomed. Opt.* **17**, 036007.
Jung, S. Y., Ahn, S., Nam, K. H., Lee, J. P. & Lee, S. J. (2012). *Int. J. Cardiovasc. Imaging*, doi:10.1007s10554-012–0029-1.
Kim, G. B. & Lee, S. J. (2006). *Exp. Fluids*, **41**, 195–200.
Lee, J. Y., Ji, H. S. & Lee, S. J. (2007). *Physiol. Meas.* **28**, 1149–1162.
Lee, S. J., Jung, S. Y. & Ahn, S. (2010). *Biosens. Bioelectron.* **25**, 1571–1578.
Lee, S. J. & Kim, G. B. (2003). *J. Appl. Phys.* **94**, 3620–3623.
Lee, S. J. & Kim, G. B. (2005). *J. Appl. Phys.* **97**, 064701.
Lee, S. J., Kim, G. B., Yim, D. H. & Jung, S. Y. (2009). *Rev. Sci. Instrum.* **80**, 033706.
Meinhart, C. D., Wereley, S. T. & Santiago, J. G. (2000). *J. Fluid Eng.* **122**, 285–289.
Mendis, S., Puska, P. & Norrving, B. (2011). Editors. *Global Atlas on Cardiovascular Disease Prevention and Control.* Geneva: World Health Organisation Press.
Nesbitt, W. S., Westein, E., Tovar-Lopez, F. J., Tolouei, E., Mitchell, A., Fu, J., Carberry, J., Fouras, A. & Jackson, S. P. (2009). *Nat. Med.* **15**, 665–673.
Poelma, C., Heiden, V., Hiereck, B. P., Poelmann, R. E. & Westerweel, J. (2010). *J. R. Soc. Interface*, **7**, 91–103.
Samarage, C. R., Carberry, J., Hourigan, K. & Fouras, A. (2012). *Exp. Fluids*, **52**, 617–631.
Sawhney, K. J. S., Dolbnya, I. P., Scott, S. M., Tiwari, M. K., Preece, G. M., Alcock, S. G. & Malandain, A. W. (2011). *Proc. SPIE*, **8139**, 813908.
Shojima, M., Oshima, M., Takagi, K., Torii, R., Hayakawa, M., Katada, K., Morita, A. & Kirino, T. (2004). *Stroke*, **35**, 2500–2505.
Smith, M. L., Long, D. S., Damiano, E. R. & Ley, K. (2003). *Biophys. J.* **85**, 637–645.
Snigirev, A., Snigireva, I., Kohn, V., Kuznetsov, S. & Schelokov, I. (1995). *Rev. Sci. Instrum.* **66**, 5486–5492.
Sugii, Y., Nishio, S. & Okamoto, K. (2002). *Physiol. Meas.* **23**, 403–416.
Tsuruta, H., Brennan, S., Rek, Z. U., Irving, T. C., Tompkins, W. H. & Hodgson, K. O. (1998). *J. Appl. Cryst.* **31**, 672–682.
Vennemann, P., Kiger, K. T., Lindken, R., Groenendijk, B. C., Stekelenburg-de Vos, S., ten Hagen, T. L., Ursem, N. T., Poelmann, R. E., Westerweel, J. & Hierck, B. P. (2006). *J. Biomech.* **39**, 1191–1200.
Vennemann, P., Lindken, R. & Westerweel, J. (2007). *Exp. Fluids*, **42**, 495–511.
Yabashi, M., Yamazakia, H., Tamasakub, K., Goto, S., Takeshitaa, K., Mochizuk, T., Yonedac, Y., Fumkawa, Y. & Ishikawa, T. (1999). *Proc. SPIE*, **3773**, 2–13.